2019
Team 343
Problem A

Analysis of deep space radiation protection

Abstract

This paper analyzes various options for spacecraft to prevent radiation in deep space (the spacecraft is set to a cylindrical shape with a base radius of 5.42m, a height of 10.84m, and a volume of approximately $1000m^3$). We propose a solution based on both superconducting magnetic shielding and passive protection, which has a total weight of 16.53 tons, and the superconducting material is BSCCO-2212 with a density of $1.8954g/cm3$.

It is an attempt to find the relatively feasible configuration for blocking high energy particles, which can be deflected by electromagnetic field. Computer simulation was used to calculate the efficiency of possible magnetic field structures in 8 plans, and one of the schemes is considered to be superior (80% of high-energy particles can be shielded by superconducting magnetic field with strength B=10T, thickness L=2 m). The blind zone of the magnetic field structure is considered, and an aluminum plate with a radius of 2 m and a thickness of 10 mm is mounted on the top of the spacecraft. In addition to setting the superconducting magnetic shielding field to deflect high-energy particles, we cover the spacecraft with a 3.75 mm aluminum plate to absorb gamma rays.

The findings show that in this scheme can block 94% of high-energy electrons with energy not exceeding 4Gev/n and 98% of γ-rays with a frequency of 10^{20} Hz. In addition, possible problems such as the damage of the strong magnetic field to the human body and the explosion of SCRs are also considered.

Contents

1 Introduction

1.1 Background

Cosmic radiation has negative effect on peoples health. It may lead to the damage of astronauts' genetic material and destroy the normal physiological function of human body. In some cases, the cosmic radiation can cause fatal diseases (leukemia, cancer). Therefore, cosmic radiation is supposed to be an essential issue in manned space flight.[1]

1.2 Cosmic radiation environment

Cosmic radiation consists of two parts: high-energy particle and high-frequency electromagnetic radiation(γ-ray).

High-energy particle is the main components, accounting for approximately 98%. It comes mainly from Earth's Radiation Belts (ERBs), Solar Cosmic Radiation (SCRs), and Galaxy Cosmic Rays (GCRs) [2]. SPEs and GCRs are major threats to astronaut safety in deep space exploration of manned spaceflight.

According to NASA reports [3]. GCRs are stable high-energy particle background sources with a radiation dose of 0.6 Sv/a and particle energy of about 1 GeV/n. SPEs are powerful source of particle transients, and the intensity and energy spectrum of each SPE is different. Picture 1 shows the GCR proton spectrum at solar minimum and solar maximum [4].

1.3 Radiation prevention method

Nowadays, the main approaches in cosmic radiation protection are the passive protection (the surface is thickened with radiation resistant materials) and magnetic active protection.

The traditional passive protection methods can effectively reduce the influence of high frequency electromagnetic radiation. However, this method appears to have little effect in high-energy particle. Therefore, the active protection

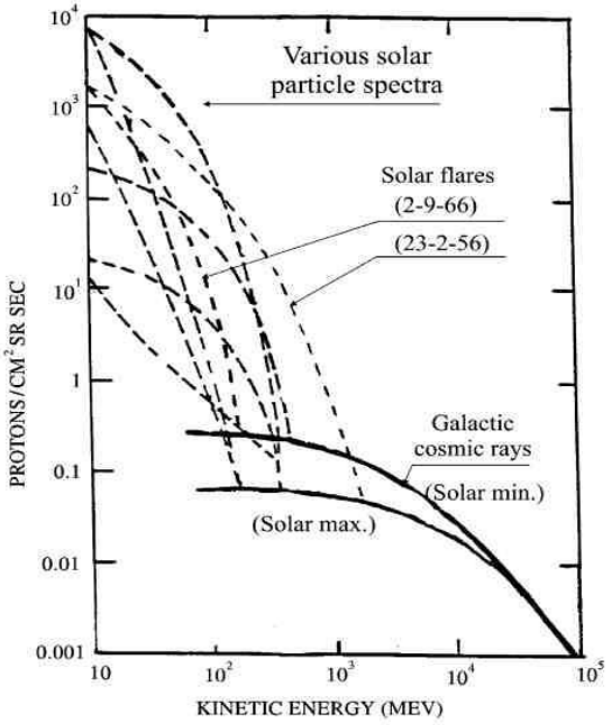

Figure 1: the GCR proton spectrum at solar minimum and solar maximum [4]

is supposed to be apply for high-energy particle protection. Magnetic protection is to form a magnetic field on the surface of the spacecraft which changes the trajectory of particle by Lorentz force.

Nowadays, with the development of superconducting technology, the magnetic protection has become the hotpots of researches.

2 Assumptions and Symbols

2.1 Assumptions

1. Cosmic radiation is uniform from all direction

2. The mass and volume of light insulating materials and refrigeration device can be neglected.

3. Virtually all the particles in the cosmic radiation are positively charged

4. The magnetic field in the shielding area is uniform, and the magnetic field strength in the non shielding area is zero

5. The second radiation of high energy particles is not considered

2.2 Notations

The primary notations used in this paper are listed in **Table 3.3.2**. There can be some other notations to be described in other parts of the paper.

Symbol	Definition
B	magnetic field intensity
L	Magnetic field thickness
H	the height of the protection area
q	Electric quantity of charged particles
γ	Lorentz Factor
θ	Angle (throwing angle) between incident direction of charged particles and shielding magnetic field
m_0	Static mass of charged particles
T	Kinetic energy of charged particles
$T_{C/O}$	The minimum kinetic energy (up to kinetic energy) required to designate point p through the protection zone.
r_0	the outer diameter of the shielding area
r_p	the radius of the thicken area in the top end of protection area
r_i	the radius of the protection area

3 Model

In previously research [4], Hoffman had already studied this problem. He proposed a ring magnetic field configuration.

It is composed of two nested concentric cylinders. The small cylinder is the protection area (protected area). The area between the large and small cylinders is full of magnetic field. The two ends of the whole structure are called the end cover area and the middle is called the barrel area.

However, passive protection was not considered in this structure. Besides, some part of the magnetic field configuration cannot block the cosmic radiation effectively. In this paper, we decided to build the model combined both the passive protection and active protection based on the Hoffmans structure, which was proved to have better results in cosmic radiation protection under finite mass and volume.

We designed the protection area which is similar to the Huffuman. The height H of the protection area is equal to the bottom diameter$D$. Therefore, in order to

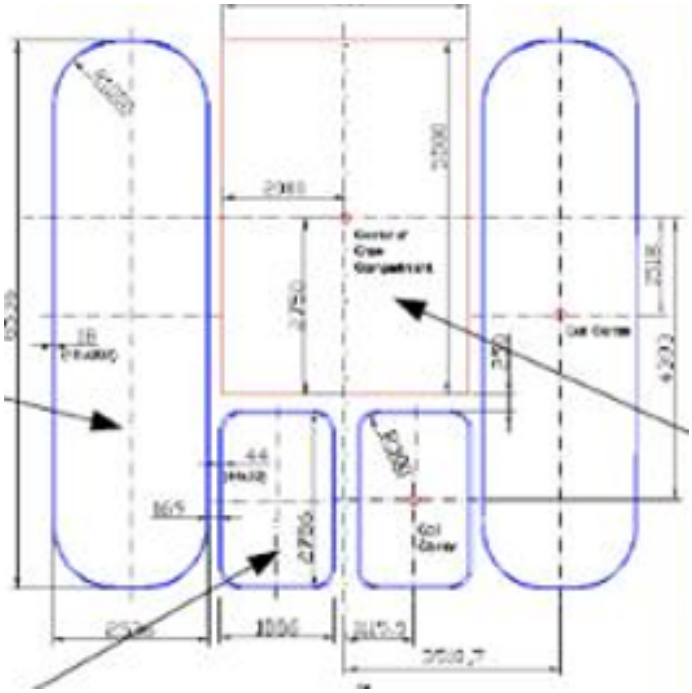

Figure 2: the Hoffman structure [3]

reach the volume requirement of $1000m^3$, we designed

$$H = D = 10.84m$$

3.1 magnetic active protection

3.1.1 Principle of deflection

The motion of high-energy charged particles (GCRs/SCRs) in the shielding magnetic field is mainly affected by Lorentz force, and the influence of non-electromagnetic force can be neglected in the cosmos. Furthermore, because of the high energy the particles in GCRs/SCRs, it is necessary to consider the relativistic effect.

Therefore, the equation of motion of charged particles in the shielding magnetic field is

$$m\frac{dv}{dt} = qv \times B$$

$$v = \frac{dr}{dt}$$

$$m = m_0 * \gamma$$

Here m, q,v, and$r$ are the relativistic mass, charged electric quantity, moving speed, and position vector of the charged particle, respectively;$m_0$is the rest mass

of the particle; γ is the Lorentz factor; B is the shielding magnetic field strength at r.

Under the effect of Lorentz force, the charged particles appear to do approximately circle motion on the plane of the vertical shielding magnetic field. The radius of gyration is also called the Larmor radius. The expression is [5]

$$r_L = \frac{\gamma m_0 v_\perp}{qB}$$

$$v_\perp = vsin\theta$$

θ is the angle between the charged particle entering direction of v and the shielding magnetic field$B$.

Assuming that the shielding magnetic field thickness is L, when $L >= 2r_L$, the charged particles will be almost completely shielded. When $L < 2r_L$, part of the charged particles are shielded by the magnetic field.

It can be seen from the above formula() that when the kinetic energy of the shielding magnetic field B and the kinetic energy of GCRs/SCRs are constant, the deflection effect of shielding magnetic field is similar for elements with atomic number $Z \geq 2$ which have the approximately equal ratio m_0/q. Therefore, in this paper, H and He elements are selected as typical GCRs/SCRs particles.

With the given the energy spectrum of GCRs / SCRs, the shielding efficiency mainly depends on the configuration of shielding magnetic field. According to the way the magnetic field deflects the particle motion and the Hoffman model [4], in this paper, we considers two magnetic field setting methods as shown in Figure 2:

The left picture shows the annular magnetic field structure, and the right picture shows the linear magnetic field structure. Both structures effectively block

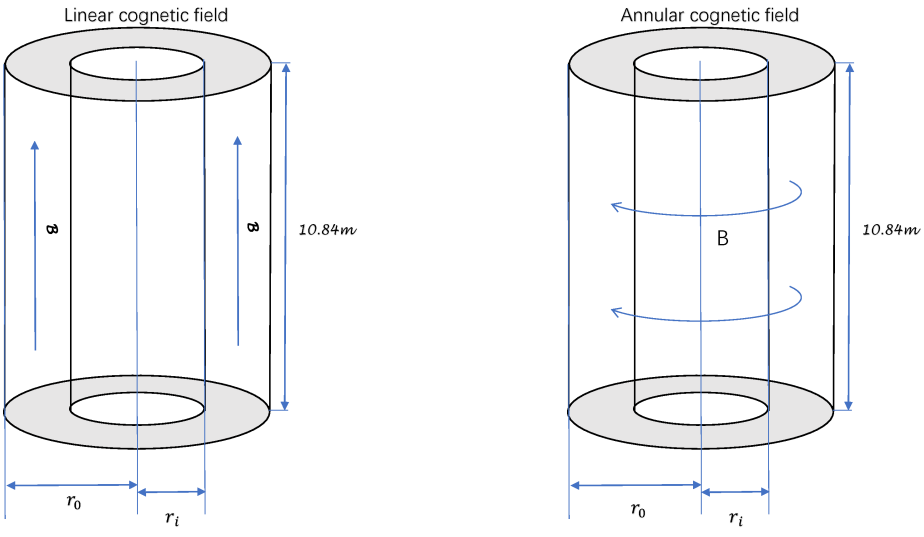

Figure 3: Schematic diagram of the magnetic field protection structure

the side GCRs/SCRs particles, but have virtually no protective effect in the direction of the top cover. We discussed the two basic structures below and then combine the two structure (with some protection in the direction of the top cover).

3.1.2 Basic structure of shielding magnetic field

1. Linear magnetic field structure

In linear magnetic field structure, the magnetic field between the large and small cylinders is linear type.

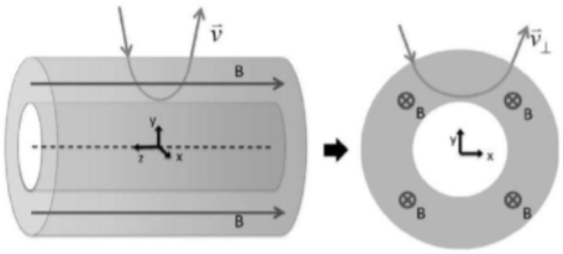

Figure 4: Linear shielded magnetic field structure [6]

For the particles incident on the side of barrel, figure 4 shows the motion orbit of charged particles in the shielding area and the protection area. The velocity of particles perpendicular to magnetic field. The azimuth angle between the velocity of charged particles and the magnetic field is defined as α.

In the shielded area, the electrons make a curve motion because of the Lorentz force, and the charged particles in the protection zone make a linear motion.

Here, we define the cut-off kinetic energy $T_{C/O}$ as the minimum kinetic energy required for incident particles to pass through the shielded magnetic field to enter the protection area,

The deflection of charged particles on the way is divided into two categories:

In the first type, particles with kinetic energy $T \leq T_{C/O}$ cannot pass through the shielded magnetic field from all azimuth angle ($0 \leq \ \leq 180$) .

In the second category, particles with kinetic energy $T > T_{C/O}$ can pass through the shielded magnetic field from some azimuth angle.

In conclusion, $T_{C/O}$ is the minimum kinetic energy required to pass the magnetic field. The moving orbit cut-off kinetic energy $T_{C/O}$ is called the limit orbit, and the radius of the orbit corresponding to the shielding zone is called the critical Larmor radius $r_{L,0}$. [7]

Assume that the magnetic field thickness is L and the magnetic induction intensity is B. The velocity of the incident particle is V, the amount of charge is

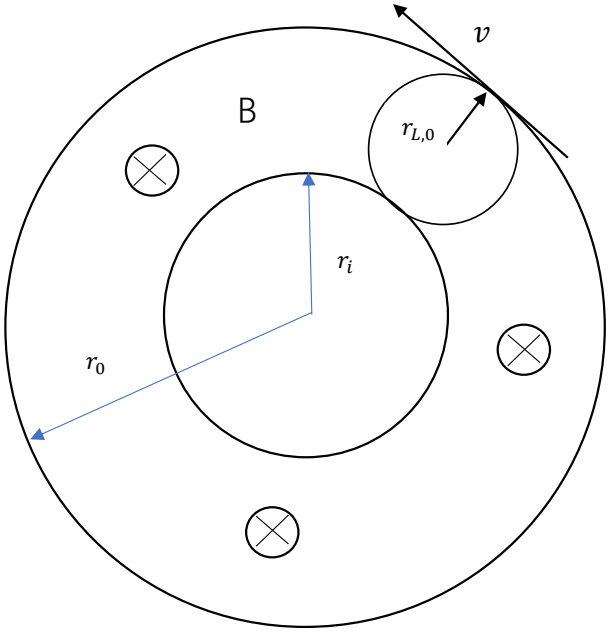

Figure 5: Motion track of charged particles in the shielded areas

q, and the static mass is m_0. In order to prevent the particle from entering the protection zone

$$r \leq r_{L,0}$$

$$2 * r_{L,0} = L$$

$$\gamma = \sqrt{1 - v^2/c^2}$$

$$T = m_0 c^2 (\gamma - 1)$$

Therefore:

$$B \geq 2 \times \frac{T/C^2 + m_0}{ql}$$

If we obtain the particle type, energy, the magnetic field thickness and the minimum magnetic field strength, the minimum B can be calculated as:

$$B = 2 \times \frac{T/C^2 + m_0}{ql}$$

However, the flux of magnetic field in the two end cover area is reduced to zero. Therefore, the high-energy charged particles incident from the two ends of the cover area can enter the protection area without limitation.

2. annular shielded magnetic field structure and cut-off kinetic energy

As shown in Figure 2(a), the annular magnetic field structure is opposite to the linear magnetic field structure:

The helical magnetic field structure can deflect the charged particles and make the particles move in the direction around the spacecraft. According to past research [7], the annular magnetic field structure and the linear magnetic field structure have virtually the same results for the deflection of charged particles.

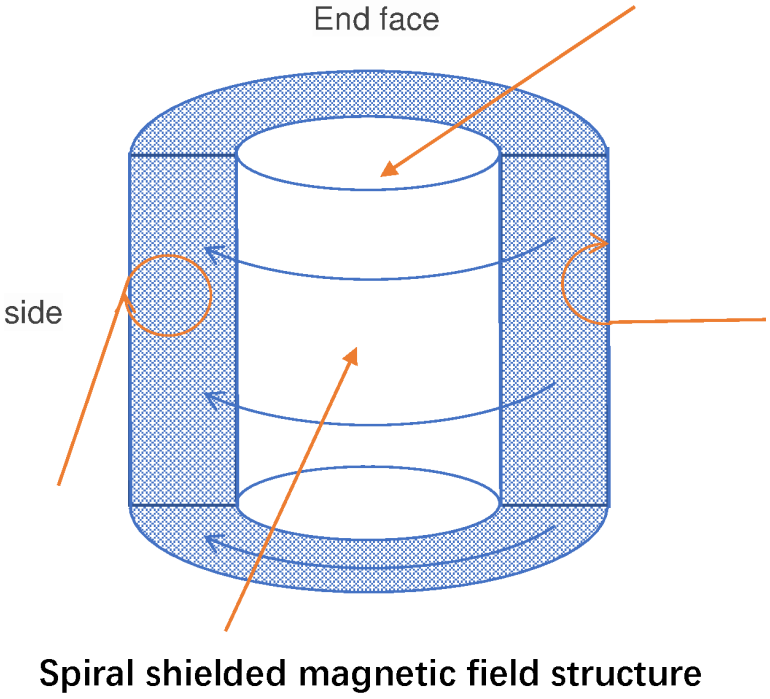

Figure 6: Motion track of charged particles in the shielded and protected areas

However, the charged particles from one end can still enter the protection area with little restriction.

Since the annular magnetic field structure and the linear magnetic field structure, they can deflect the particles in different directions. This means that the mutual deficiencies can be compensated for by improving and combining the two basic structures. In 3.2, we will combine the two basic structures for analysis in the next section.

3.2 Design and analysis of shielded magnetic field structure

When the magnetic field strength B is large enough $B \geq 2 \times \frac{\frac{T}{C^2}+m_0}{ql}$ the radiation particles of the entering the protection zone mainly come from the end cover area. In this chapter, eight combined magnetic field structures are designed to reduce the radiation from the end cover area. In addition, we investigate the overall shielding efficiency of the combination of different basic magnetic field structures.

The shielding effect of shielding magnetic field structure, strength B and thickness L on typical GCRs H and He (2GeV-4GeV) particles was compared and the protective effects of H and He spectra in typical GCR events were further investigated.

3.2.1 Eight combined shielding magnetic field structures

Different magnetic field structures in the barrel and end cover areas will produce different shielding effects.

Figure 7(1) shows the magnetic field structure proposed by Hoffman [4] in 2005. In the top side of the Hoffmans structure, the particles can enter the protection area. With some improvements, figure 7(2) shows the two end sides can prevent the particles effectively. However, some charged particles can pass the magnetic field from the barrel area in figure 7(4).

Therefore, we apply the different structures in two different areas (the barrel and the end cover area) respectively and design the eight combined structures

Magnetic field configuration		1	2	3	4	5	6	7	8
Barrel zone	Bit pattern	ring		Linear type		Linear type		ring	
	direction	e_θ		$-e_z$		$-e_z$		e_θ	
	axial length	z	z+2l	z	z+2l	z	z+2l	z	z+2l
	Thickness	L	L	L	L	L	L	L	L
End cap area	Bit pattern	ring		ring		Linear type		Linear type	
	direction+z	e_θ		e_θ		$-e_r$		$-e_r$	
	direction+z	$-e_\theta$		$-e_\theta$		$-e_r$		$-e_r$	
	Radius	r_i	r_i+L	r_i	r_i+L	r_i	r_i+L	r_i	r_i+L
	Thickness	L	L	L	L	L	L	L	L

Table 1: Shielding magnetic field structure

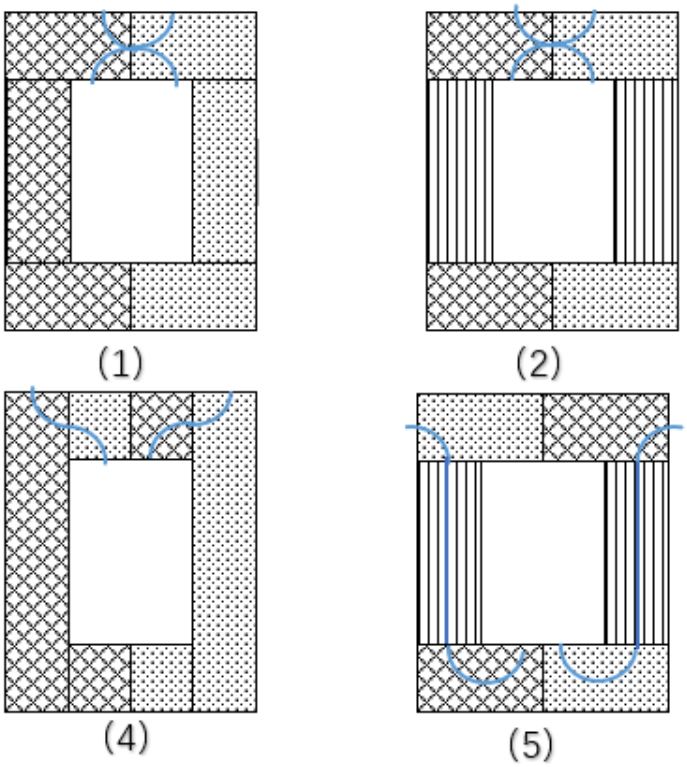

Figure 7: Weak area of different structures

Where r_i represents the radius of the protection zone, Z represents the length of the protection zone, L is the thickness of the shielding magnetic field, e_z is the axial direction of the barrel zone, e_r is the radial direction of the barrel zone, and e_θ satisfies the right hand annular relationship.

3.2.2 Investigate shielding effectiveness of eight different magnetic field structures

In this part, we use the computer to stimulate the movement of the particle in different magnetic field structure.

In order to evaluate the shielding effect of the magnetic field, we adopt the method used by Hoffman [4] to investigate the shielding efficiency of the magnetic field by calculating the reduction rate η. The calculation formula is:

$$\eta = 1 - n_{in2}/n_{in1}$$

Here, n_{in1} and n_{in2} represent the number of particles entering the protection zone without and with a magnetic field respectively.

Since the initial particles (GCRs) are Isotropy outside the shielded magnetic field, we assume that the particles are incident at a spherical source. The paper

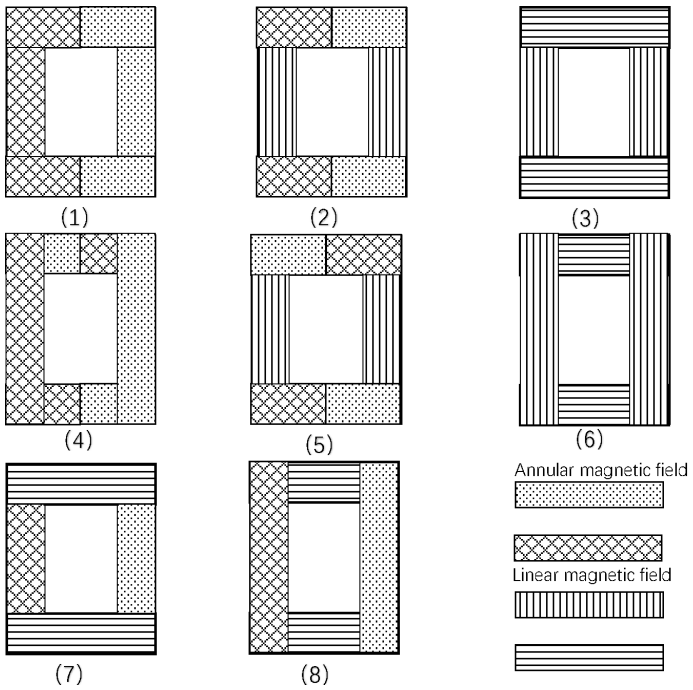

Figure 8: Eight different structrues of magnetic field

uses a computer simulation method to simulate the incident particle source.

The sphere radius is set to 6 m, and 20,000 points (10000 H particles, 10000 He particles) are randomly selected on the sphere, with random direction and kinetic energy(2GeV-4GeV). The calculation step $\Delta t = T/100$, (T is the cyclotron period of charged particles)

The different results of reduction rate η of the eight structures are shown in figures 8, 9, and 10:

3.2.3 Select the best structure

In figure 8,9,10, we can find that the structure 2 has the relatively higher reduction rate in most cases. Therefore, the structure 2 is supposed to be the most

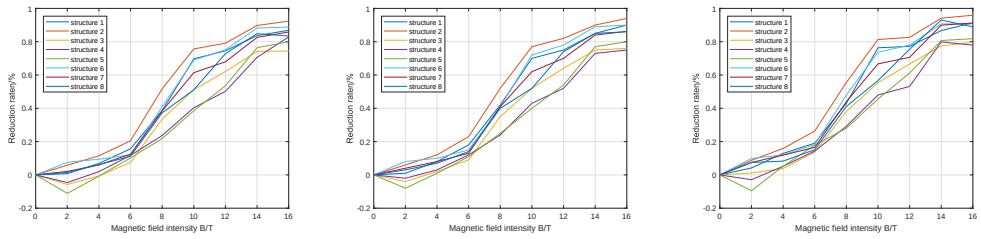

Figure 9: Schematic diagram of the magnetic field protection structure

effective structure.

When B is relatively low ($B = 2T$), the reduction rate η can be negative in some structures, which proves that the magnetic field may have negative effect on the radiation protection.

Besides, the reduction effect η increases together with B. it rises rapidly after $B = 4T$, until $B = 10T$. Then the shielding effect remains almost unchanged.

The shielding effect increases quite slowly with the increase of L, when consider the size of the structure, we can choose $L = 2m$ Therefore, we will select the magnetic field thickness $L = 2m$ and the magnetic field strength $B = 10T$ as the standard in the design of structure. In this condition(B=10T,L=2m),the structure 2 can prevent about 81% of the radiation.

3.3 Passive protection of materials

In the above analysis, it is found that the all these structures of magnetic field protection are not perfect due to some blind area of shielding magnetic field. Some charged particles may enter the protection area because of the effect of Lorenz force, which seems to reduce the protection effect in some areas of the magnetic field. In addition, the high-frequency electromagnetic radiation(-ray) cannot be blocked by the magnetic field. Therefore, the passive protection approaches need to be applied.

3.3.1 Magnetic shielding blind zone protection

In 3.2, structure 2 was selected as a magnetic shielding structure.

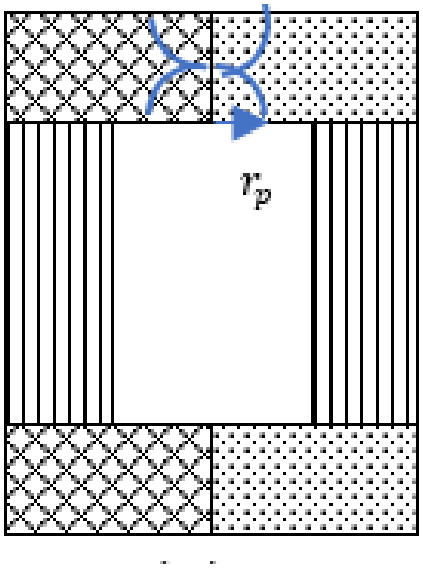

Figure 10: Motion track of charged particles in the shielded and protected areas

As shown, the solution has a blind spot on one side of the end cap region. Here the shielding efficiency is close to zero. According to document [11], The absorption of high-energy charged particles by metals can be expressed by equations:

$$\phi(E) = \phi'(e)\frac{S(E')}{S(E)}exp(\sigma_A d)$$

Where d is the thickness of the shielding material, is the macroscopic absorption cross section of the particle,$\phi(E), \phi'(e)$respectively represent the particle flux of the extra-chamber energy and the energy entering the cabin reduced to E, $S(E), S(E')$ represent the barrier power of the shielding material (here is aluminum) for the two energy particles.

The energy before and after the particles penetrate the shielding material has the following relationship:

$$E = R^{-1}[R(E) + d]$$

Where $R(E)$ is the range of the particle with energy E, represents a negation function. If the particle range is less than d, it is blocked in the shielding material. We hope that the aluminum layer can shield 90%$\frac{S(E')}{S(E)} = 0.1$energy particles in the end cap area. Calculated:

$$d10mm$$

This means that the end cap area needs to be mounted with a 10 mm thick aluminum plate to shield 90% of the high energy particles on the area of L^2.

3.3.2 Cosmic gamma ray protection

High-frequency electromagnetic radiation can be absorbed by metals, according to the attenuation equation of γ rays in metals [9]:

$$I = I_0 exp(-\mu x)$$

Here I_0 represents the initial intensity of the ray, I represents the residual strength after passing through a section of the metal with a thickness x, and μ is the attenuation coefficient. Generally, μ is a function of the atomic coefficient of the substance and the frequency of the rays. According to [8], the frequency of the γ ray in the cosmic radiation is about 10^20Hz. Table 2 shows the attenuation coefficient μ. of γ ray in some common metals [10]

By comparing the attenuation coefficient and density of different metals, it is supposed that aluminum is the most suitable as a passive protective layer material. (Aluminum is competent attenuation coefficient for ray absorption and has relatively lighter density)

In order to protect the safety of astronauts, at least 95% of γ rays are supposed to be absorbed:

$$\frac{I}{I_0} = exp{-\mu x} \leq 0.05$$

material	thickness δ/mm	Attenuation coefficient μ	Linear absorption coefficient κ
aluminum	0.2	0.8	1
aluminum	0.5	0.8	1.04
aluminum	1	0.8	1.08
iron	0.2	1.2	1.27
iron	0.5	1.2	1.82
iron	1	1.2	3.32
copper	0.2	1.8	1.43
copper	0.5	1.8	2.46
copper	1	1.8	6.05
Tantalum	0.2	7.5	4.48
Tantalum	0.5	7.5	42.5
Tantalum	1	7.5	1808

Table 2: Comparison of attenuation coefficients of four materials with different thicknesses

Therefore, the material thickness x:

$$x \geq -ln(0.05)/mu$$

The attenuation coefficient of the aluminum material is = 0.8, and x >= 3.75 mm is obtained. Therefore, if 95% of gamma rays are to be absorbed, the surface of the spacecraft must cover at least 3.75 mm of aluminum.

4 Model solving and analysis

4.1 Model solving

In general, the protective layer of the spacecraft consists of an active protective structure and a passive protective structure. The protection zone is a cylinder with a radius of 5.42 m and a height of 10.84m.

4.1.1 Active protection structure

The active protection structure consists of two main parts: the end cover area and the barrel area,

1. The end cover area In order to form the Annular magnetic field in the end cover area, we design this coil structure:

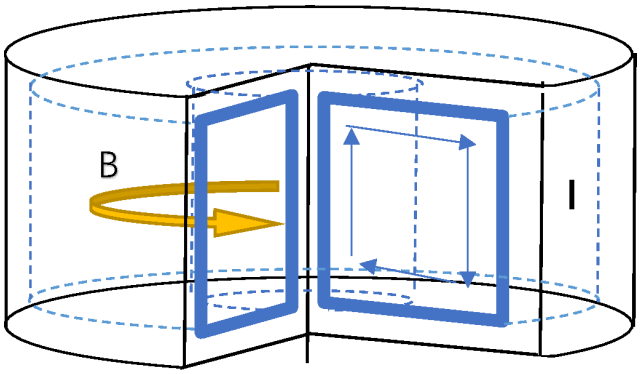

Figure 11: Superconducting coil at both ends

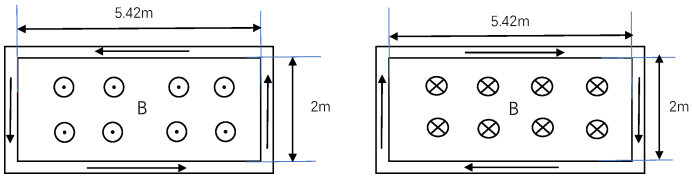

Figure 12: Superconducting coil at both ends

The rectangular coil has a length of 5.42m and a width of 2m. The opposite coils have opposite current directions, and each end cover area has 20 rectangular coils.

2. The barrel area

In the barrel region, in order to form the linear magnetic field, the structure of coils is:

There are 20 cylinder of light insulating material with the radius of 1m on the side of the protection zone. And in each cylinder, there are four turns of coils on.

Among them, the internal structure of each cylinder is:

The left figure is the model of superconducting coils. The figure in the right is the light insulating cylinder.

In each cylinder, the distance between the coils is 2m.

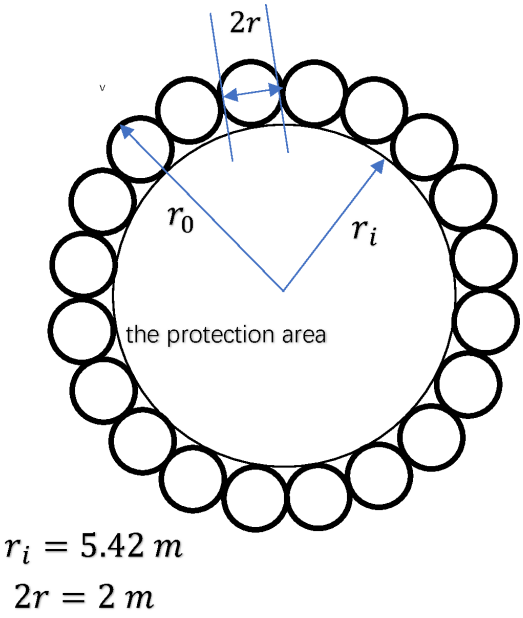

Figure 13: Single side coil and Light insulating cylinder

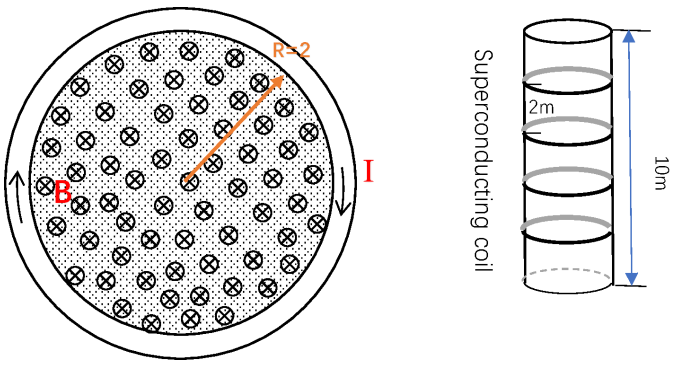

Figure 14: Top view of side coil

4.1.2 Passive protection structure

The passive protective structure consists of two main parts: the thickening area in the top and the bulkhead of spacecraft. 1. The bulkhead of spacecraft

The surface of the spacecraft is covered with 3.75 mm of aluminum. 2. the thickening area in the top:

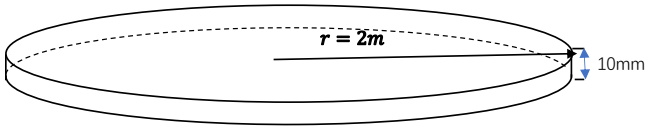

Figure 15: thickened area in the top end

the aluminum plate on one side of the cover was thicker. The aluminum plate at top is set to 10 mm and a circular area having a radius of 2 m at the center of the end cap.

In addition, in order to fix the superconducting coil, light foam is used to fill between the superconducting coils.

In conclusion, the structure diagram of the spacecraft protective layer is:

4.2 Quality Analysis

The mass of the spacecraft's protective layer includes the mass of the excitation coil in the end cap area, the mass of the excitation coil in the barrel, the mass of the anti-gamma ray aluminum layer in the flight cabin and the mass of the thickened aluminum layer.

For a superconducting coil, the spatial magnetic field it excites can be calculated by Biot-Savart Law:

$$\vec{B} = \int_L \frac{\mu_0 I}{4\pi} \frac{\boldsymbol{dl} \times \vec{e_r}}{r^2}$$

Where μ_0 is the permeability in vacuum, I is the current in the superconducting coil, and r is the distance from a point in the space to the coil. dl is the micro-element of the superconducting coil segment.

We select the Superconducting material BSCCO-2212 to make the coil. According to document [8], the density of BSCCO-2212 $\rho_{BSCCO-2212} = 1.8954 g/cm^3$. Under the condition of 77K , the superconducting critical current density $J = 7100 A/mm^2$.

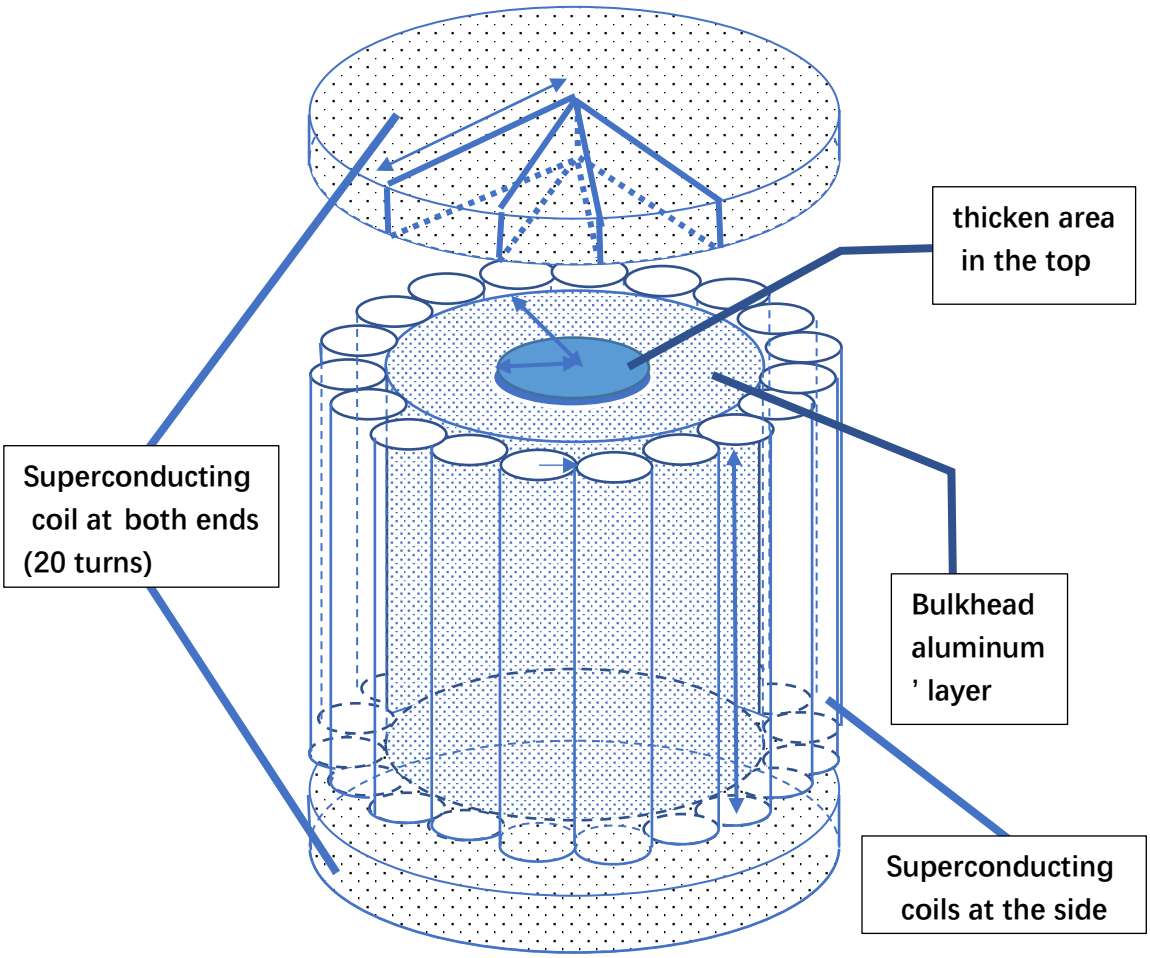

Figure 16: Overall structure of the spacecraft

1. Mass of end cap area excitation coil

The magnetic field strength at both ends of the protection zone is $B = 10T$, and the magnetic permeability in vacuum is $\mu_0 = 4\pi \times 10^{-7} T * m/A$. The current intensity I_1 can be calculated according to Biot-Savart Law.

Therefore, the critical surface area of a superconducting wire is:

$$S_1 = I_1/J$$

Therefore, the mass of a single-turn superconducting coil is:

$$m_1 = S1 * 2 * \pi * r_0 * \rho_{BSCCO-2212}$$

Where r_0 is the outer diameter of the shielding area Calculated that $m_1 = 99.041kg$ There are 20 coil columns on the side of the protection zone, and each coil column has 4 turns of coils. The end cap area excitation coil total mass:

$$M_1 = 20 * 4 * m_1 = 3.961 * 103kg$$

2. Mass of barrel area excitation coil

The magnetic field strength on the side of the protection zone is $B = 10T$. According to Biot-Savart Law, The current intensity I_2 can be calculated. Therefore, the critical surface area of a superconducting wire is:

$$S_2 = I_2/J$$

The mass of a single-turn superconducting coil is:

$$m_1 = S_1 * 2 * \ * r_0 * \rho_{BSCCO-2212} = 83.8672kg$$

There are 20 coil columns at each end of the protection zone, and each coil column has 1 coil. The end cap area excitation coil total mass:

$$M_2 = 20 * m_2 = 20 * 2 * \pi * S2 * r_0 * \rho_{BSCCO-2212} = 6.709 * 103kg$$

3. Mass of flight cabin anti-gamma ray aluminum layer

A layer of 3.75mm aluminum layer is evenly mounted on the surface of the protection zone to prevent gamma rays. The quality of the aluminum layer is:

$$M_3 = 2 * \pi * ri * L_y + 2 * \pi * ri^2 * {}_v * \Delta h$$

Where r_i is the radius of the protection area, L_y is the length of the guard zone, ${}_v$ is the density of aluminum, and Δh is the thickness of the aluminum layer. Brought into the calculation:

$$M_3 = 5.5065 * 103kg$$

4. Mass of Aluminum layer thickened part

The thickened part of the aluminum layer is a circular area with a radius of $r = 2m$, and the thickness is $\Delta L = 10mm$, so the added mass is:

$$M_4 = \pi * r^2 * v * (L - \Delta h)$$

Obtained $M_4 = 339.29kg$ Therefore, the total mass of the guard is

$$M = M_1 + M_2 + M_3 + M_4 = 16.53 * 103kg = 16.53t$$

4.3 Analysis of protection effect

After considering some possible factors, we mathematically calculate the protection effect of the system on high-energy charged particles and γ rays.

1. Protection efficiency for high-energy charged particles

According to Figure 9, it can be found that the structure selected in this paper (structure 2) can be shielded at $B = 10T$.

About 87% of high-energy charged particles. On this basis, an aluminum plate with a radius of $2m$ and a thickness of $10mm$ was installed on the top of the protection zone. According to [11], the $10mm$ aluminum plate can basically protect all high energy particles below $2Gev/n$. Therefore, the defense efficiency against high-energy charged particles:

$$\sigma_1 = [0.87 * (S_0 - S) + S]/S_0 * 100\%$$

Among them,S_0 is the surface area of the protection zone, and S is the area of the thickened zone. Calculated: High-energy charged particle defense efficiency $\sigma_1 = 89\%$

2. Protection efficiency against gamma rays

According to the above analysis, in the case where the aluminum plate is 3.75 mm covering the entire surface of the protection zone, the γ-ray defense efficiency σ_2 is 95%.

However, in actual conditions, the thickness of the aluminum plate with a circular area of $2m$ is $10mm$, which will increase σ_2. Therefore, the defense efficiency against high-energy charged particles:

$$\sigma_1 = [0.95 * (S_0 - S) + S]/S_0 * 100\%$$

Among them, S_0 is the surface area of the protection zone, and S is the area of the thickened zone. Calculated: High-energy charged particle defense efficiency $\sigma_1 = 95.3\%95\%$

4.4 Feasibility analysis

We have also considered other feasibility related issues:

1. The average ambient temperature of the Earth to Mars is 153K, which can reach 77K under the action of refrigerant. Meet the operating temperature of the BSCCO superconducting coil.

2. The magnetic field generated by the superconducting coil B=10T is harmful to the human body. However, the structure of the coil is analyzed, and the magnetic fields generated by the superconducting coils symmetric about the central axis of the protection zone in the protection zone cancel each other out. In addition, a small anti-magnetic coil can be added to the spacecraft to ensure safety. (The magnetic field does not harm the astronauts)

3. The lightweight insulating plastic is filled between the superconducting coils to enhance the flight stability of the spacecraft.

4. If the spacecraft encounters an SCR outbreak during flight, it can enhance the shielding capability by temporarily increasing the current.

5 Model advantages and disadvantages

5.1 Advantages

1. The active protection scheme is set to reduce the weight of the spacecraft's outer casing.

2. Consider the blind zone of active protection and make up for it by means of local passive protection.

3. Compare 8 different magnetic field configuration schemes, choose a better solution, and enhance the shielding ability of radiation.

4. The computer simulation method was used to analyze the influence of magnetic field strength B and magnetic field thickness L on the shielding effect, and the better B and T were selected.

5.2 Disadvantages

1. Protection against high energy uncharged particles is not considered.

2. The critical current density of BSCCO is not large enough and the operating temperature is low. Therefore, the magnetic field B generated by the magnetic shield may not reach 10T.

6 Conclusions

In this paper, various options for spacecraft to prevent deep space radiation are analyzed (the spacecraft is set to be cylindrical with a base radius of 5.42 meters, a height of 10.84 meters and a volume of about $1000m^3$). For the relatively feasible structures for blocking high-energy particles, the efficiency of possible magnetic field structures in the eight schemes are calculated by computer simulation, of which scheme 2 is considered superior (87% of high-energy particles can be shielded by superconducting magnetic fields with a strength of $B = 10T$ and a thickness of $L = 2m$). Considering the blind area of the magnetic field structure, an aluminum plate with a radius of 2 m and a thickness of 10 mm is installed on the top of the spacecraft. In addition to setting superconducting magnetic shielding fields to deflect high-energy particles, we also covered the spacecraft with a 3.75mm aluminum plate to absorb gamma rays. The results show that the scheme can block 89% of high energy electrons with energy less than 2Gev/n and 95% of gamma rays with frequency of 10^20 Hz.

References

[1] Xu Zhenhua. Radiation environment and radiation protection in manned space [C] / / abstracts of the 16th Symposium on space life of the Chinese Academy of space sciences. 2005

[2] Townsend L W, Wilson J W, Shinn J L, et al. Human exposure to large solar particle events in space[J]. Advances in Space Research, 1992, 12(2-3): 339-348.

[3] Hoffman J, Fisher P, Batishchev O. Use of superconducting magnet technology for astronaut radiation protection[J]. Final Report for NIAC Phase I Contract CP, 2005: 04-01.

[4] Hoffman J, Fisher P, Batishchev O. Use of superconducting magnet technology for astronaut radiation protection[J]. Final Report for NIAC Phase I Contract CP, 2005: 04-01.

[5] Griffith D J , Ruppeiner G . Introduction to Electrodynamics[J]. American Journal of Physics, 1981, 49(12):1188-1189.

[6] `http://www.chinatex.org/`

[7] Zheng Hongxia. Study on the Mechanism of Magnetic Shielding Protection against Space Radiation [D]. Nanjing University of Aeronautics and Astronautics, 2018.

[8] Tajmar M, Hense K, Marhold K, et al. Weight Measurements of HighTemperature Superconductors during Phase Transition in Stationary, NonSta-

tionary Condition and under ELF Radiation[C]//AIP Conference Proceedings. AIP, 2005, 746(1): 1290-1297.

[9] Zhang Lei, Jia Mingchun, Gong Junjun, Xia Wenming. Study on a fast method for calculating -ray mass attenuation coefficient based on MCNP [J]. journal of naval university of engineering, 2018,30(05):106-112.

[10] Chen Panxun. Experimental Measurement of X-ray Attenuation Coefficients of Different Metal Materials for Different Energies [A] ... Annual Scientific Report of China Institute of Engineering Physics (2002)[C]: Editorial Department of Annual Scientific Report of China Institute of Engineering Physics, 2002:2.

[11] Ye Zonghai. On the shielding and protection of high-energy charged particles [A]. Space Exploration Committee of the Chinese Society of Space Science. Proceedings of the 16th Academic Conference of the Space Exploration Committee of the Chinese Society of Space Science (II) [C]. Space Exploration Committee of the Chinese Society of Space Science: China Society of Space Science, 2003:14.